BeBeC-2020-D15

CHARACTERIZATION OF ENGINE JET NOISE IN FLIGHT CONDITIONS USING ADVANCED ACOUSTIC IMAGING METHODS

Q. Leclère[1], N. Aujogue[1,2], A. Dinsenmeyer[1,3], J. Antoni[1], E. Julliard[2]
[1]Univ Lyon, INSA-Lyon, LVA EA 677, F-69621, Villeurbanne, France
[2]Airbus Operations S.A.S, Acoustics Department, Toulouse, France
[3]Univ Lyon, École Centrale de Lyon, LMFA UMR 5509, F-69134 Écully, France

Abstract

This paper presents some applications of advanced acoustic imaging techniques to flight test data. Engine jet is one of the main sources contributing to cabin noise in cruise flight conditions. The use of fuselage microphone arrays offers the possibility to extract information about the noise source mechanisms responsible for the jet noise, in terms of localization, quantification and directivity. Previous studies present beamforming space-frequency maps allowing the localization of main sources of noise along the jet axis as a function of the frequency. Beamforming is a robust acoustic imaging method, well adapted to the measurement conditions of fuselage microphones (low SNR), however it suffers from several drawbacks (space resolution, source correlations) that limits the analysis possibilities. In the present work, some advanced acoustic imaging techniques are implemented in order to overcome limitations inherent to beamforming. Deconvolution and identification methods are used to draw 1D and 2D source maps, offering the possibility to go deeper in the source characterization and to draw some physical interpretations about jet noise source mechanisms.

1 INTRODUCTION

The application of acoustic imaging methods to aircraft flight test measurements is a challenging task. Plane microphones are generally fixed on the external face of the fuselage, consequently strongly affected by the pseudo-sound (pressure variations of hydrodynamic nature) generated by the turbulent boundary layer (TBL). At usual Mach numbers ($M \approx 0.85$), standard Signal to Noise ratios are often negative, classically lying between -10 and -20dB. However, previous studies [1] show the possibility of getting some information about the acoustic sources generated by the engine jet, mainly using beamforming approaches. If well adapted to such

difficult application cases, because of its robustness, beamforming is however known to have a poor spatial resolution, making it difficult to conduct a fine analysis of source mechanisms. In the last decades, numerous advanced imaging methods have been developed in different application fields (deconvolution approaches in aeroacoustics, holography in vibroacoustics ..., see [2, 3] for recent detailed reviews) but generally lose in robustness when increasing in separation power. However, some advanced methods seem to have reached a robustness level allowing an application to such difficult cases as flight tests. The aim of this paper is to demonstrate the ability of two advanced imaging methods, namely CLEAN-PSF (for CLEAN based on point spread functions [4]) and SBF (for Sparse Bayesian Focusing [5]) to tackle such complex data, and to show their added value as compared to conventional beamforming.
The first section of the paper is dedicated to a brief description of the different acoustic imaging methods used in the following of the paper. A second part describes the test configuration: the microphone array, the specific denoising techniques used to separate the acoustic field from the TBL, and some preliminary results about the pressure field on the microphone array. The last three sections are dedicated to 3D, 1D and 2D acoustic imaging analysis, respectively. The preliminary 3D analysis allows to roughly validate the source location in the space. Then, the 1D and 2D analysis show some interesting results with a resolution never observed up to now on such flight tests, providing new material for a deeper understanding of jet noise mechanisms on an aircraft in realistic flight conditions.
Note that for the whole paper, level, frequency and position information have been normalized for confidentiality reasons.

2 Acoustic imaging approaches

2.1 Subsonic convected Green function

Acoustic imaging methods are, most of the time, based on an analytic formulation of the acoustic propagation. Considered acoustic waves can be assumed either plane (for farfield sources) or spherical. In the latter case, candidate sources are distributed in the space and the acoustic transfer functions are considered between point sources and microphones. In the present work, the acoustic propagation is affected by the velocity of the medium with respect to the aircraft. Considering a uniform flow along the x direction $\mathbf{U} = M.c\mathbf{x}$ ($M < 1$), the acoustic pressure radiated by a point source at point $(0,0,0)$ is given by

$$g(x,y,z) = \frac{exp^{-ik\rho}}{4\pi R}, \text{ with } R = \sqrt{x^2 + (1-M^2)(y^2+z^2)} \text{ and } \rho = \frac{R - Mx}{1-M^2} \tag{1}$$

As an illustration, the convected Green function is drawn in 1 at 500Hz, Mach .85, for the configuration studied in the present work (see section 3 for more details). It is clear that, for such flow speeds, the wavenumber content of the measured pressure field is strongly distorted. The position of the source along the direction of the flow is very sensitive, it has to be taken into account when analysing acoustic imaging results.

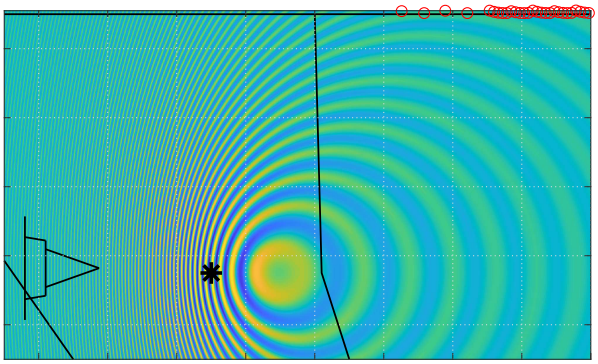

Figure 1: Convected Green function mapped in a horizontal plane (x,y) at the height of the microphone array for a point source at the z position of the engine axis, at a normalized frequency $f_n = 1.66$, M=0.85. Black $*$: source location, red o: microphone locations. The leading and trailing edges of the wing, as well as the rear part of the engine, are drawn in solid black.

2.2 Beamforming coherence

The beamforming coherence is a measure of the correlation between the measured pressure field and the pressure fields resulting from each candidate source position. A way of calculating this indicator is as follows

$$\gamma_i^2\left(\mathbf{S_{pp}}\right) = \frac{\mathbf{g}_i^H.\mathbf{S_{pp}}.\mathbf{g}_i}{\|\mathbf{g}_i\|^2.\mathrm{Tr}\left(\mathbf{S_{pp}}\right)}, \tag{2}$$

where the j^{th} term of $\mathbf{g}_i$ given by the convected Green function (1)

$$\mathbf{g}_i|_j = g(x_i - x_j, y_i - y_j, z_i - z_j)$$

This way of assessing the coherence is however limited by the use of measured auto-spectra at the denominator. In aeroacoustics, autospectra are known to be highly disturbed by flow noise, and are usually not used for acoustic imaging. An alternative way of calculating a correlation indicator based only on cross-spectra is :

$$\Gamma_i^2\left(\mathbf{S_{pp}}\right) = \frac{\Lambda\left\{\mathbf{g}_i\mathbf{g}_i^H\right\}^H.\,\Lambda\left\{\mathbf{S_{pp}}\right\}}{\|\Lambda\left\{\mathbf{g}_i\mathbf{g}_i^H\right\}\|.\,\|\Lambda\left\{\mathbf{S_{pp}}\right\}\|}, \tag{3}$$

where $\Lambda\{\mathbf{X}\}$ stands for the vertical concatenation of columns of matrix $\mathbf{X}$ omitting diagonal terms. Γ_i^2 is simply a correlation coefficient between measured cross-spectra and cross-spectra of the pressure field generated by source #i. Note that the numerator of Eq. (3) is equal to that of Eq. (2) setting to zero the diagonal terms (similarly to diagonal removal approaches). However,

the normalisation term at the denominator is different, it does not use measured autospectra. If measured cross-spectra perfectly match the cross-spectra generated by source #i, Γ_i^2 will be equal to 1, whatever the level of uncorrelated noise.

2.3 Clean-PSF

Clean-PSF [4] is a matching pursuit-like algorithm, that assumes the independence between sources. Source positions and amplitudes are found iteratively by maximizing a residual beamforming map. In the present work, the maximisation is realized on a beamforming coherence map, based on the formulation (3). The source amplitude at the position j maximising the coherence is obtained as follows :

$$q^2 = \frac{\Lambda\left\{\mathbf{g}_j\mathbf{g}_j^H\right\}^H . \Lambda\left\{\mathbf{S_{res}}^{(n)}\right\}}{\left\|\Lambda\left\{\mathbf{g}_j\mathbf{g}_j^H\right\}\right\|^2}, \text{ with } j = \text{argmax}_i\left(\Gamma_i^2\left(\mathbf{S_{res}}^{(n)}\right)\right) \tag{4}$$

Note that this estimation of the source squared amplitude is also estimated only from cross-spectra, similarly to Γ_i^2. This way of estimating q^2 does not guarantee its positivity from a mathematical point of view. However, from a physical point of view, this positivity is expected and a negative result is a sign of poor correlation. The residual CSM is estimated at each iteration as follows :

$$\mathbf{S_{res}}^{(n+1)} = \mathbf{S_{res}}^{(n)} - q^2\mathbf{g}_j\mathbf{g}_j^H \quad , \quad \mathbf{S_{res}}^{(0)} = \mathbf{S_{pp}}, \tag{5}$$

the identified source amplitude q^2 obtained at each iteration being stored into the clean map.

2.4 Sparse Bayesian Focusing (SBF)

SBF [5] belongs to the class of inverse problems, quantifying all source strengths at once, contrarily to beamforming based methods (including CLEAN-PSF) that considers individually each candidate source. It is an under-determined problem because the number of potential source points is often much greater than the number of available microphones. Additional information has to be injected in the problem so as to define a unique and physically meaningful solution. In SBF, this information is enforced by considering a prior on the source amplitudes following a generalized Gaussian pdf. This prior gives more credibility to amplitudes equal to zero, encouraging sparse solutions. SBF is implemented using an iterative reweighted least squares algorithm, using a Bayesian regularization at each iteration :

$$\mathbf{S_q}^{(n+1)} = \mathbf{A}\mathbf{S_p}\mathbf{A}^H, \quad \text{with } \mathbf{A} = \left(\mathbf{G}\mathbf{W}^{(n+1)}\right)^{+\eta} \tag{6}$$

where the $^{+\eta}$ denotes the Tikhonov-regularized pseudo-inverse, the regularization parameter η being determined using a Bayesian criterion [6]. The right diagonal weighting matrix W at iteration $(n+1)$ is defined by the result at iteration n:

$$\mathbf{W}^{(n+1)}|_{i,i} = \left(\mathbf{S_q}^{(n)}|_{i,i}\right)^{1/2}, \quad \text{with } \mathbf{W}^{(0)} = \mathbf{Id}$$

3 Test cases, array configuration and denoising

3.1 Measurement configurations

Two different measurement configurations are investigated in the present work:

- cruise: cruise conditions, engine at full power, $M = 0.85$,
- idle: background noise measurement configuration, engine at idle speed, $M = 0.8$.

3.2 Microphone distribution

33 microphones are distributed on the left side of the fuselage of the aircraft, behind the wing, specifically designed to characterize the engine jet noise (see Fig. 2). The microphone array

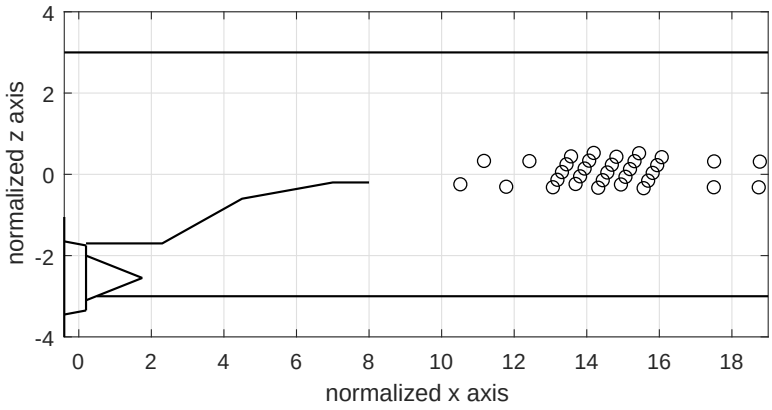

Figure 2: Microphone array distribution on the fuselage.

is mainly distributed along the x-axis, but also has some spreading over the z-axis ; the width over height ratio being equal to 10, approximately. Some Point Spread Functions(PSF) in a vertical plane containing the jet axis are drawn in Fig. 3, for two frequencies and two source positions, at a Mach number of .85. Considering the microphone distribution, the lobes are logically elongated along z, the resolution in one given direction being related to the dimension of the array along the same direction. The effect of the convection is also visible on the PSFs. The resolution of the microphone array depends on the position of the source : the PSF is more compact for a source located downstream. The location of secondary lobes is also affected by the flow : lobes in the downstream direction are much closer to the main lobe than the upstream ones.

3.3 Denoising

For each configuration, signals are recorded synchronously during 60s at 32kHz, CSMs are calculated with a resolution of 4Hz (overlap 66%). Microphone signals are strongly disturbed by the TBL developed on the fuselage. A reference based denoising approach is implemented in this work so as to remove as much as possible this contribution. References used for the

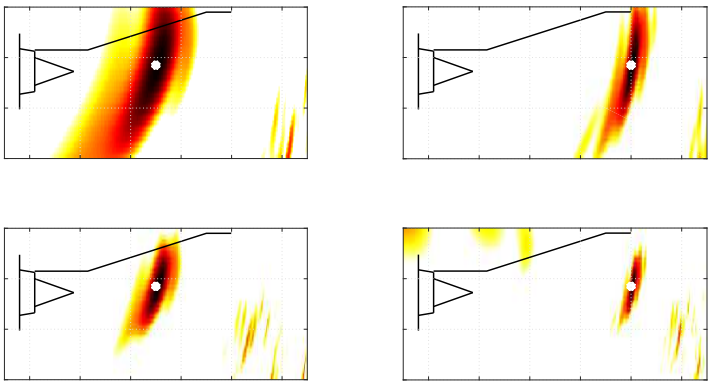

Figure 3: Point Spread Functions at M=0.85 for sources at two different normalized frequencies (top: 1.66, bottom: 3.33) and two different positions (left/right). Source positions are materialized by white dots. Color scale dynamic 20dB.

denoising are 9 microphones located inside the cabin, so as to focus on the part of the noise that is efficiently transmitted through the fuselage skin. The denoised CSM is obtained as follows :

$$\mathbf{S_{pp}}^{ref} = \mathbf{S_{pr}} . (\mathbf{S_{rr}})^{-1} . \mathbf{S_{pr}}^{H}, \tag{7}$$

where $\mathbf{S_{pp}}^{ref}$ is the referenced CSM, representing the part of the CSM that is coherent with the references. Note that this approach can simply be interpreted as a generalization of the Coherent Spectrum to the multiple reference case (cf. [7]).

Average autospectra for the two measurement configurations are drawn in Fig. 4, before and

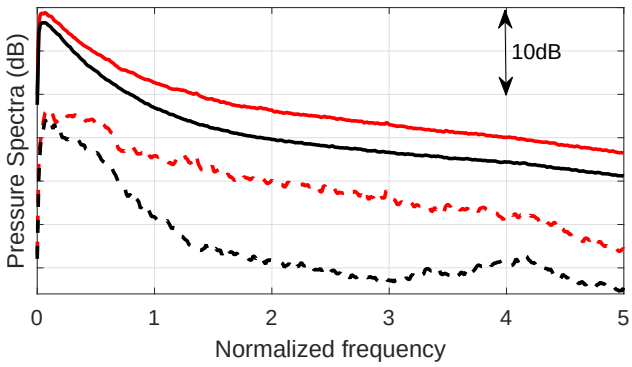

Figure 4: Acoustic pressure spectra for configuration cruise (red) and idle (black). Raw averaged autospectra (solid), averaged denoised autospectra (dashed).

after reference based denoising. On the whole frequency range, the TBL dominates the pressure spectra. It can be seen that the TBL contribution is a few dBs louder for the cruise configuration than for the idle one. The reason of this difference can be explained neither by the contribution of the engine jet, nor by the slightly lower Mach number. The authors suspect that the nature

of the TBL slightly differs between the two configurations, because of the loss of flight altitude encountered during the measurement at idle speed. The difference is more important when looking at the denoised spectra : the denoising process removes 8dB on a wide frequency range for the cruise configuration, and 13-14dB for the idle configuration.
The spectra for the whole microphone are represented on space-frequency maps in Fig. 5, for cruise and idle configurations, before and after denoising. Concerning maps obtained before denoising, differences between cruise and idle configurations are mainly due to the differences between TBL properties during the two configurations, as explained above. The effect of jet noise is however slightly visible for raw spectra of the cruise configuration, and well highlighted when looking at denoised spectra. Some specific radiation patterns appear, with some energetic lobes whith central frequencies sliding towards the high frequency range when looking at downstream microphones. Those patterns are likely related to broadband shock associated noise (BBSAN, [8]), due to the interaction between the shear layer and the shock cells. Similar results have been obtained in a previous work [1]. When looking at denoised spectra of the idle configuration, a component appears in the normalized frequency range $[3-4.5]$, for upstream microphones (normalized x position in $[11-16]$). This component is also seen on average spectra (Fig. 4), with a hump centered around the normalized frequency 4. This component is an external acoustic source that contributes significantly to the cabin noise (references used for denoising are microphones located in the cabin). In order to identify the source of this component, the acoustic imaging methodologies, initially developed to characterize engine jet noise, are also implemented in the following for the idle configuration.

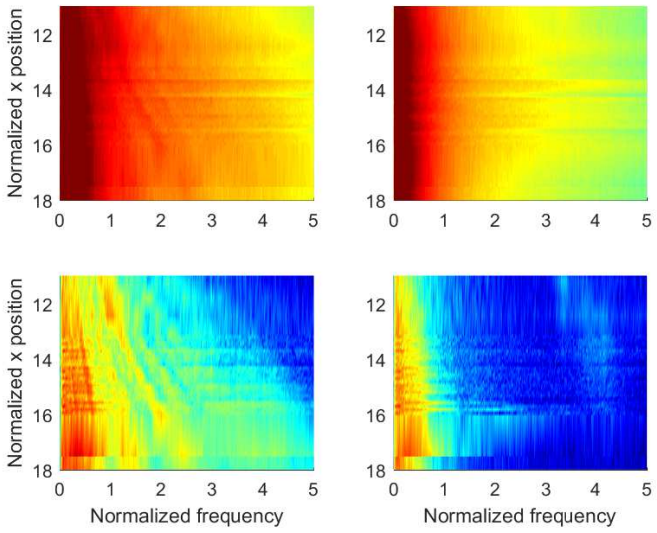

Figure 5: Denoised acoustic pressure spectra for configuration cruise (left) and idle (right), raw (top) and denoised (bottom), as a function of the microphone normalized x-axis location. Color range 30dB.

4 3D beamforming coherence maximization

The aim of this section is to present a preliminary analysis of the source field, with a minimum a priori information about the source location. More than 5.10^5 candidate sources are distributed on a 3D regular grid of normalized dimensions $13 \times 5 \times 5$, centered on the region of interest (behind the engine). At each frequency, the beamforming coherence is calculated for all candidate sources. The position maximizing this function is retained at each frequency, and maximum coherences are then summed over a wide frequency range (for instance, the resulting value at a position maximizing the coherence for 2 frequencies with coherence values of 0.9 and 0.8 will be 1.7).
Resulting 3D maps are presented in Fig. 6 for cruise and idle measurements. Source positions for which at least one maximum has been found are materialized by dots, whose colors and diameters are proportional to the sum over the frequencies. This kind of representation gives a qualitative indication of the zones that are more likely to contain main acoustic source terms.

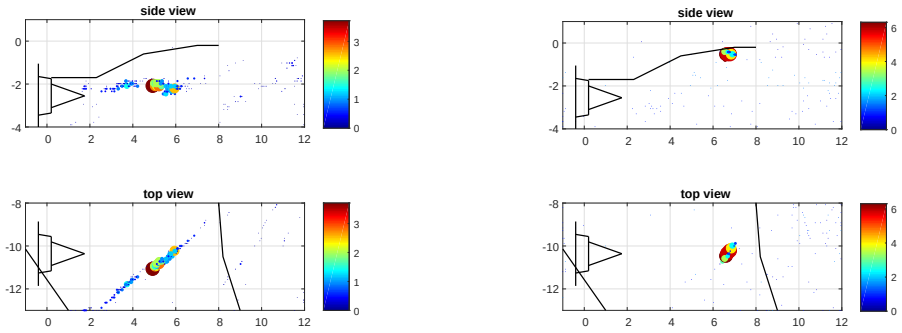

Figure 6: 3D beamforming coherence maximisation, wideband results for cruise (left) and idle (right) conditions. Top : side views ((x,z) plane projection with normalized units). Bottom : side views ((x,y) plane projection with normalized units).

For the cruise configuration, during which the engine runs at a standard operating point, the sources are found mainly around the jet axis, behind the engine, as expected (see Fig. 6, left). The source distribution is along a horizontal line, directed towards the microphone array. This is an artifact due to the poor resolution of the array along the y direction. However, the maximum values of this distribution are correctly found at the actual y and z position of the jet. These observations are important for the following steps (the 1D and 2D acoustic imaging) for which some hypotheses are assumed on the y or z positions of the sources.
Concerning the idle configuration, the engine operates at idle speed. No jet noise is expected, however, it has been observed in the previous section that an acoustic component is still noticeable in the high frequency range (see Fig. 4). The 3D coherence maximization is also realized, so as to determine the location of this source (see Fig. 6, right). A very compact source zone is highlighted, unexpectedly also located at the y position of the jet axis. However, the x and z position differs, it is found at the height of the wing, just behind the engine pylon. This source might be related to the wake of the pylon, at the junction with the wing.

5 1D Analysis

Considering preliminary results obtained using 3D beamforming maximization, and also considering the geometry of the microphone array, a 1D source region is defined on a line along the x dimension. For the cruise configuration, this line corresponds to the jet axis. For the idle configuration, the z position is changed, it is defined at the same height as the source highlighted with 3D beamforming (just below the trailing edge of the wing).
An interest of the 1D analysis is that space-frequency maps of the source can be easily drawn. Such maps are drawn in Figs. 7, obtained with the 3 different acoustic imaging methods introduced in 2.
The hypothesis of source location along a line is very strong, and inevitably leads to model bias that has to be kept in mind at the interpretation step.

Concerning results for the cruise configuration, 3 different frequency bands can be distinguished. Below $f_n = 1.3$, the result is strongly disturbed by the effect of the TBL, that is not efficiently suppressed by the denoising step presented in section 3.3. The contribution of the TBL, also clearly seen for the results obtained for the idle configuration, appears on the beamforming coherence as a continuous line varying between $f_n = 0.2$ and $f_n = 1.3$ for source points located at dowstream to upstream positions. This is an artifact due to the energy of the convective peak of the TBL that is projected on the source map. However, when comparing cruise and idle configuration, it is clear that some additional sources related to the engine are also contributing in this frequency range. The analysis is however complicated by the mixing with the contribution of the TBL.
Above $f_n = 1.3$ and below $f_n = 2$ a source structure clearly appears, especially on maps obtained with SBF. At least four sources are highlighted, regularly spaced, between the normalized x_n positions 4 and 8. These positions could correspond to the shock cell structure of the jet. Other sources appear more downstream, for normalized positions after $x_n = 8$. However, their interpretation through sparse imaging results is more difficult.
In the high frequency range, above $f_n = 2$, results seem to be also very significant, making appear a source structure frankly different from the one observed between $f_n = 1.3$ and 2. Two very close sources are separated by SBF between $x_n = 5.5$ and 6, while three sources are identified by CLEAN-PSF between $x_n = 5$ and 6. These differences can be explained by two reasons: the first one is that there is a strong difference in the hypothesis of SBF and CLEAN: the former can deal with correlated sources while the latter makes the assumption that sources are uncorrelated. The second reason is that the two imaging approaches can react differently to the bias error induced by the projection of sources on a line.
For the idle configuration, the strong source already highlighted using 3D beamforming coherence maximisation clearly appears above $f_n = 3$, and for x_n around 6.5. SBF shows two very close mixed sources, while once again CLEAN finds at least 3 sources, with a kind of main source with few sidelobes. These differences between SBF and CLEAN results can be explained by the two reasons already given just before.

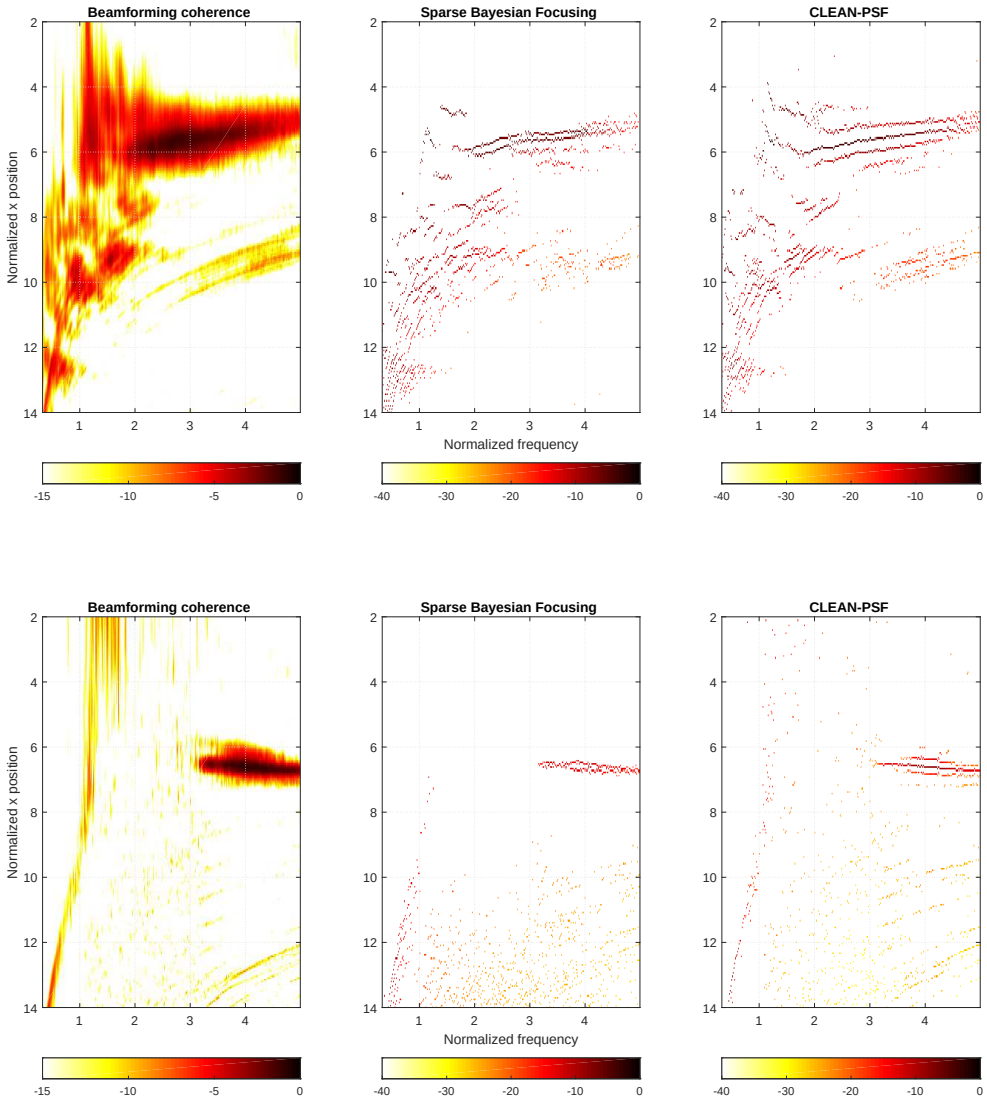

Figure 7: Top: 1D acoustic imaging results, cruise configuration , normalized (y,z) positions (-10.3,-2.4). Bottom: 1D acoustic imaging results, idle configuration, normalized (y,z) positions (-10.3,-0.5).

6 2D Analysis

In order to relax a little bit the strong observation bias due to a 1D source distribution, a 2D source distribution is considered in this section. This relaxation has two counterparts: the first one is that space-frequency maps are not possible any more, the second one is that the number of source points in the source distribution is much higher, increasing significantly the computational effort. Considering the 1D analysis presented in the previous section, in which the source

structure has exhibited different aspects as a function of the frequency, some 2D source maps are given in Fig. 8 and for the cruise configuration, integrated in the normalized frequency ranges $[1.33, 2]$ and $[2.66, 3.33]$.

Concerning the map obtained between $f_n = [1.33, 2]$ (Fig. 8), discrete source locations are

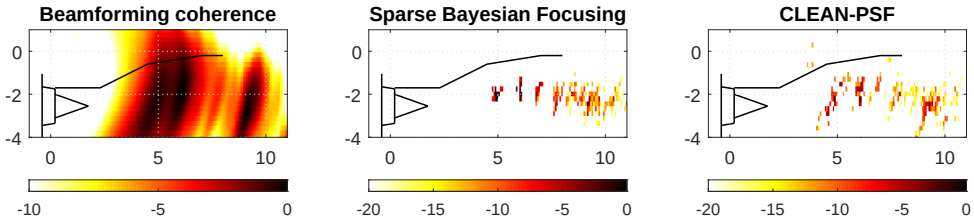

Figure 8: 2D acoustic imaging results, cruise config., normalized frequency range [1.33 2].

found between $x_n = 5$ and 8, confirming the 1D results. As it is the case for the 1D analysis, the 2D source distribution obtained with SBF seems better defined than the one from CLEAN. Sources seem to be more extended spatially along the vertical axis, this is however doubtlessly due to the resolution of the microphone array that is finer on the horizontal direction. However, the center of gravity of each source seems to be slightly higher than the engine axis.

The 2D source map is also drawn for the frequency range $f_n = [2.66, 3.33]$ for the cruise con-

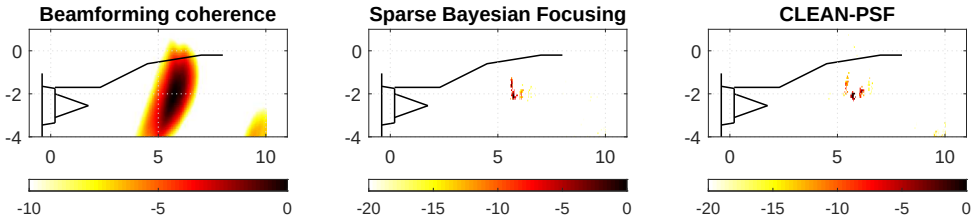

Figure 9: 2D acoustic imaging results, cruise config., normalized frequency range [2.66 3.33].

figuration. In this frequency range, the 1D analysis found a very compact source area between $x_n = 5$ and 6. Two very close sources were found using 1D-SBF, two close sources are also found on the 2D-SBF results, however separated by a small distance over the vertical axis. The x-axis position of these two sources is found just between the two first sources identified in the previously analysed frequency range $[1.332]$. Concerning results obtained with CLEAN, the source distribution is much similar to SBF than for the 1D case, maybe thanks to the observa-

tion bias that has been reduced with 2D images. However, differences still appear, because of the different hypothesis of the two methods on source correlation.

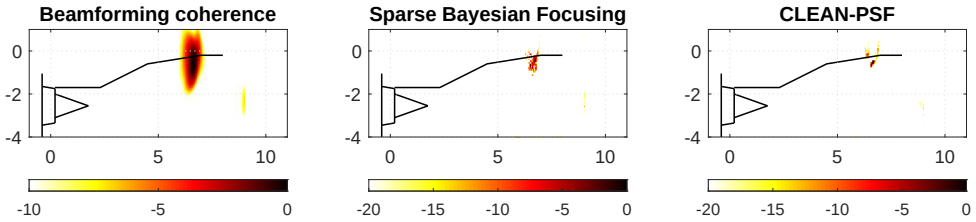

Figure 10: 2D acoustic imaging results, idle conf., normalized frequency range [3.33 4.66].

The same 2D analysis is conducted for the idle configuration, in the frequency range of the source highlighted in the previous sections ($f_n = [2.66, 3.33]$). As expected, the source is found at a vertical position significantly higher than the engine axis. The position of the source corresponds geometrically very well to the position of the rear junction between the pylon and the wing. The source distribution, although very compact and similarly centred for SBF and CLEAN, still exhibit small differences than can be explained by the diffraction effects (source very close to the wing and its trailing edge), affecting differently the two methods.

7 CONCLUSIONS

The aim of this paper was to demonstrate the ability of some advanced acoustic imaging techniques to achieve valuable results even in the particularly challenging situation of flight tests. Two different methods have been compared to standard beamforming: CLEAN-PSF, and SBF, that have been implemented in the frame of 1D and 2D analyses. Some interesting observations have been made on the studied case, either concerning the broadband shock associated noise, but also about the presence of a strong aeroacoustic source observed at the idle configuration. A perspective of future work is to associate the identified source distributions to the real mechanisms of noise generation, which is not an easy task concerning the observation bias induced by the hypotheses of the methods.

Acknowledgements

This work was performed within the framework of the Labex CeLyA of Université de Lyon, operated by the French National Research Agency (ANR-10-LABX-0060/ANR-16-IDEX-0005), and of the Clean Sky 2 Joint Undertaking, European Union (EU), Horizon 2020, CS2-RIA, ADAPT project, Grant agreement no 754881.

REFERENCES

[1] Jerome Huber, Kevin Britchford, Estelle Laurendeau, Vincent Fleury, Jean Bulté, Amadou Sylla, and Dean Long. *Understanding and Reduction of Cruise Jet Noise at Model and Full Scale*.

[2] Q Leclère, A Pereira, C Bailly, J Antoni, and C Picard. A unified formalism for acoustic imaging based on microphone array measurements. *International Journal of Aeroacoustics*, 16(4-5):431–456, 2017.

[3] R. Merino-Martínez, P. Sijtsma, M. Snellen, T. Ahlefeldt, J. Antoni, C. J. Bahr, D. Blacodon, D. Ernst, A. Finez, S. Funke, T. F. Geyer, S. Haxter, G. Herold, X. Huang, W. M. Humphreys, Q. Leclère, A. Malgoezar, U. Michel, T. Padois, A. Pereira, C. Picard, E. Sarradj, H. Siller, D. G. Simons, and C. Spehr. A review of acoustic imaging methods using phased microphone arrays. *CEAS Aeronautical Journal*, 10(1):197–230, March 2019.

[4] P. Sijtsma. CLEAN Based on Spatial Source Coherence. In *13th AIAA/CEAS Aeroacoustics Conference, Rome, Italy, May 21-23, 2007*, pages AIAA–2007–3436, 2007.

[5] Jérôme Antoni, Thibaut Le Magueresse, Quentin Leclère, and Patrice Simard. Sparse acoustical holography from iterated bayesian focusing. *Journal of Sound and Vibration*, 446:289 – 325, 2019.

[6] A. Pereira, J. Antoni, and Q. Leclere. Empirical bayesian regularization of the inverse acoustic problem. *Applied Acoustics*, 97:11 – 29, 2015.

[7] Q. Leclere, J. Antoni, E. Julliard, and A Pintado-Peno. Consideration of estimation error in multiple coherence approaches: application to the inside/ outside coherence analysis of aircraft flight tests. In *proceedings of ISMA 2018*, Leuven, Belgium, 2018.

[8] Marcus Harper-Bourne and M Fisher. The noise from shock waves in supersonic jets. In *Proceedings of the AGARD Conference on Noise Mechanisms*, 09 1973.